

Fig. 41.2 The triplet and quartet of bound state energies (over Binding) are offset horizontally. They interleave. Similarly for the resonance peaks (over Scattering). Each resonance peak lies slightly above the corresponding bound state, both for the quartet and the triplet. All levels and resonances lie within the edges of the corresponding band (shown over Periodic) of the corresponding periodic potential.

42

Wavefunctions and Probability Distributions

The transfer matrices $T = M_1 M_2$, which were used in chapters 37 and 38, relate the amplitudes of the trigonometric/hyperbolic cosines and sines in adjacent unit cells of a periodic lattice. We make this point explicit here. Suppose unit cell i consists of two regions, 1 and 2, in which the potential is constant, as shown in Fig. 42.1. We choose $V_1 = -5.0$ eV, $V_2 = 0.0$ eV and $E > V_1$, $E < V_2$. In regions 1 and 2 of cell i and region 1 of cell $i + 1$ the wavefunctions are

$$\begin{aligned}\psi_i^1(x) &= A_i \cos kx + B_i \frac{1}{k} \sin kx, \\ \psi_i^2(x) &= C_i \cosh \kappa x + D_i \frac{1}{\kappa} \sinh \kappa x, \\ \psi_{i+1}^1(x) &= A_{i+1} \cos kx + B_{i+1} \frac{1}{k} \sin kx.\end{aligned}\quad (42.1)$$

Within each region, the value of x ranges from 0 at the left edge to $L_1 = 8.0$ Å in region 1 and $L_2 = 2.0$ Å in region 2. When the boundary conditions are imposed, we obtain the following equations:

$$\begin{pmatrix} \cos kL_1 & \frac{1}{k} \sin kL_1 \\ -k \sin kL_1 & \cos kL_1 \end{pmatrix} \begin{pmatrix} A \\ B \end{pmatrix}_i = \begin{pmatrix} C \\ D \end{pmatrix}_i, \quad (42.2)$$

$$\begin{pmatrix} \cosh \kappa L_2 & \frac{1}{\kappa} \sinh \kappa L_2 \\ \kappa \sinh \kappa L_2 & \cosh \kappa L_2 \end{pmatrix} \begin{pmatrix} C \\ D \end{pmatrix}_i = \begin{pmatrix} A \\ B \end{pmatrix}_{i+1}. \quad (42.3)$$

These equations are easily inverted

$$\begin{pmatrix} A \\ B \end{pmatrix}_i = \begin{pmatrix} \cos kL_1 & -\frac{1}{k} \sin kL_1 \\ k \sin kL_1 & \cos kL_1 \end{pmatrix} \begin{pmatrix} C \\ D \end{pmatrix}_i = M_1 \begin{pmatrix} C \\ D \end{pmatrix}_i, \quad (42.4)$$

$$\begin{pmatrix} C \\ D \end{pmatrix}_i = \begin{pmatrix} \cosh \kappa L_2 & -\frac{1}{\kappa} \sinh \kappa L_2 \\ -\kappa \sinh \kappa L_2 & \cosh \kappa L_2 \end{pmatrix} \begin{pmatrix} A \\ B \end{pmatrix}_{i+1} = M_2 \begin{pmatrix} A \\ B \end{pmatrix}_{i+1} \quad (42.5)$$

As a result

$$\begin{pmatrix} A \\ B \end{pmatrix}_i = M_1 M_2 \begin{pmatrix} A \\ B \end{pmatrix}_{i+1} = T \begin{pmatrix} A \\ B \end{pmatrix}_{i+1} \quad (42.6)$$

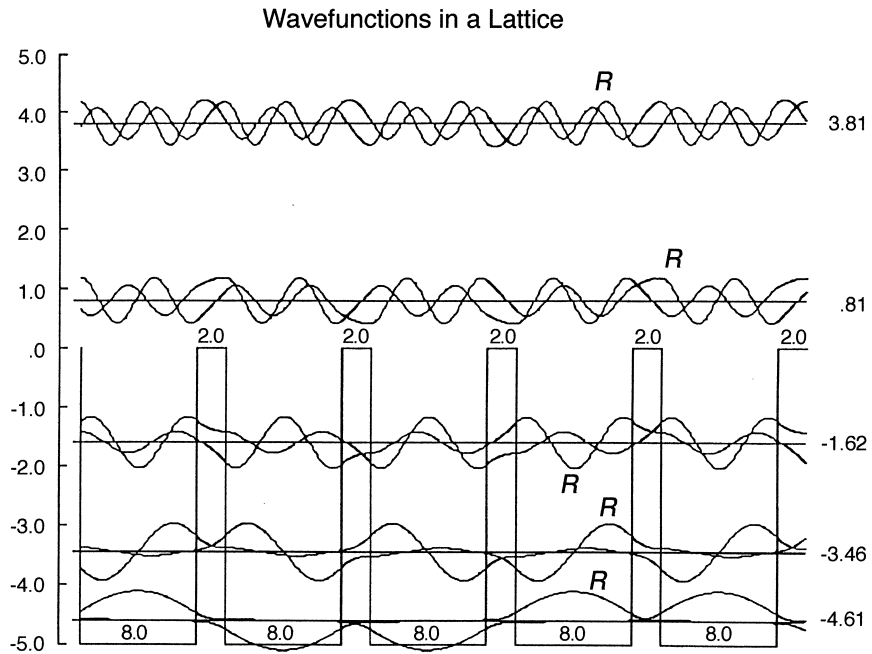


Fig. 42.1 Real and imaginary parts for one eigenstate in each of the five lowest bands of the periodic potential shown. The real parts are identified.

Remark: If we had used (A, B) as amplitudes for the right- and left-propagating exponentials e^{+ikx}, e^{-ikx} and (C, D) as amplitudes for the exponentially decaying and growing exponentials $e^{-\kappa x}, e^{+\kappa x}$, then we would have found the following relation

$$\begin{pmatrix} A \\ B \end{pmatrix}_i = K^{-1} T K \begin{pmatrix} A \\ B \end{pmatrix}_{i+1}, \quad K = \begin{bmatrix} 1 & 1 \\ +ik & -ik \end{bmatrix} \quad (42.7)$$

The quantization condition (i.e., (37.3)) is valid whether we use T or its similarity transformed version $K^{-1}TK$. However, wavefunction calculations are *much* easier with the cosine and sine basis set.

42.1 UNIT CELL PHASE SHIFT

The wavefunctions in any part of cell i and the corresponding part of cell $i + 1$ are

$$\begin{aligned}\psi_i(x) &= \begin{pmatrix} \Phi_1(x) & \Phi_2(x) \end{pmatrix}_i \begin{pmatrix} A \\ B \end{pmatrix}_i, \\ \psi_{i+1}(x) &= \begin{pmatrix} \Phi_1(x) & \Phi_2(x) \end{pmatrix}_{i+1} \begin{pmatrix} A \\ B \end{pmatrix}_{i+1} \\ &= \begin{pmatrix} \Phi_1(x) & \Phi_2(x) \end{pmatrix}_i T^{-1} \begin{pmatrix} A \\ B \end{pmatrix}_i.\end{aligned}\quad (42.8)$$

The last equation was obtained by inverting (42.6). If the amplitudes (A, B) are chosen as eigenvectors of T with eigenvalue λ , then $T^{-1} \begin{pmatrix} A \\ B \end{pmatrix} = \lambda^{-1} \begin{pmatrix} A \\ B \end{pmatrix}$.

As a result

$$\psi_{i+1}(x) = \lambda^{-1} \psi_i(x). \quad (42.9)$$

In an allowed band, $\lambda = e^{\pm i\phi}$. This means that the wavefunction in cell $i + 1$ is simply a phase-shifted version of the wavefunction in cell i . If the wavefunction in cell i is known, it can be used to construct the wavefunction in the adjacent cells. For example, if we write the wavefunctions in terms of their real and imaginary parts and choose $\lambda^{-1} = e^{i\phi}$, then

$$\psi_{i+1}^R(x) + i\psi_{i+1}^I(x) = e^{i\phi} (\psi_i^R(x) + i\psi_i^I(x)), \quad (42.10)$$

$$\begin{pmatrix} \psi^R(x) \\ \psi^I(x) \end{pmatrix}_{i+1} = \begin{pmatrix} \cos \phi & -\sin \phi \\ \sin \phi & \cos \phi \end{pmatrix} \begin{pmatrix} \psi^R(x) \\ \psi^I(x) \end{pmatrix}_i. \quad (42.11)$$

42.2 WAVEFUNCTIONS

The wavefunction in any part of cell i can be written as a linear superposition of the basis functions $\Phi_1(x), \Phi_2(x)$ in that region:

$$\psi_i(x) = A_i \Phi_1(x) + B_i \Phi_2(x), \quad (42.12)$$

where the amplitudes $(A, B)_i$ satisfy the appropriate eigenvalue equation:

$$T \begin{pmatrix} A \\ B \end{pmatrix}_i = e^{i\phi} \begin{pmatrix} A \\ B \end{pmatrix}_i.$$

To compute the unnormalized amplitudes $(A, B)_i$, we rewrite this equation as follows

$$\begin{bmatrix} t_{11} - e^{i\phi} & t_{12} \\ t_{21} & t_{22} - e^{i\phi} \end{bmatrix} \begin{bmatrix} A \\ B \end{bmatrix} = 0 \iff \begin{cases} (t_{11} - e^{i\phi})A + t_{12}B = 0 \\ t_{21}A + (t_{22} - e^{i\phi})B = 0 \end{cases} . \quad (42.13)$$

The two equations on the right are not independent. They can be used to determine A and B

$$\begin{pmatrix} A \\ B \end{pmatrix} \sim \begin{pmatrix} e^{i\phi} - t_{22} \\ t_{21} \end{pmatrix} \sim \begin{pmatrix} t_{12} \\ e^{i\phi} - t_{11} \end{pmatrix} . \quad (42.14)$$

The two expressions for the amplitudes are proportional to each other. Using the first expression, we find

$$\psi_i(x) = \frac{1}{2} \underbrace{(t_{11} - t_{22}) \cos kx + t_{21} \frac{1}{k} \sin kx}_{\psi_i^R(x)} + i \underbrace{\sin \phi \cos kx}_{\psi_i^I(x)} . \quad (42.15)$$

The wavefunctions in other regions of the i th cell are computed using the transfer matrices M_1 , M_2 , and so on (see equation (42.6)). The wavefunctions in adjacent regions are computed using the phase shift property (42.10).

In Fig. 42.1 we show wavefunctions computed for one state in each of the five lowest bands in the periodic potential shown. The real and imaginary parts of each wavefunction are plotted and are labeled with an R or an I . All wavefunctions have been normalized so that the integral of $|\psi(x)|^2$ over a unit cell is the same for each eigenfunction.

In fact, the real and imaginary parts of these wavefunctions are interchangeable. If a wavefunction obtained using the angle $-\phi$ is multiplied by i , then we obtain

$$i \times (\psi^R(x) - i\psi^I(x)) = \psi^I + i\psi^R(x) . \quad (42.16)$$

This is the wavefunction obtained using the angle ϕ and interchanging the real and imaginary parts.

The nondegenerate eigenfunctions at the edges of each band can always be made real, since the eigenvalues are $\lambda = \pm 1$. The corresponding wavefunctions are standing waves, whereas the degenerate eigenfunctions describe waves traveling to the left and right.

42.3 PROBABILITY DISTRIBUTIONS

Since the wavefunction in cell $i + 1$ is just a phase-shifted version of the wavefunction in cell i , the probability distribution in cell $i + 1$ is equal to the probability distribution in cell i :

$$P_{i+1}(x) = |\psi_{i+1}(x)|^2 = |e^{i\phi}\psi_i(x)|^2 = |e^{i\phi}|^2 |\psi_i(x)|^2 = |\psi_i(x)|^2 = P_i(x) . \tag{42.17}$$

As a result, the probability distribution is invariant from cell to cell.

In Fig. 42.2 we plot the probability distributions for one eigenstate in each of the five lowest bands of the potential shown in Figs. 42.1 and 42.2. These distributions have all been properly normalized (the integral over every unit cell is $1/N$ for each of the probabilities). Although the nodal structure of the wavefunctions is not obvious from Fig. 42.1, it is much clearer in Fig. 42.2. The number of ‘nodes’ within each well increases by one for each successive band. The energies at which the computations were done for Figs. 42.1 and 42.2 differ slightly.

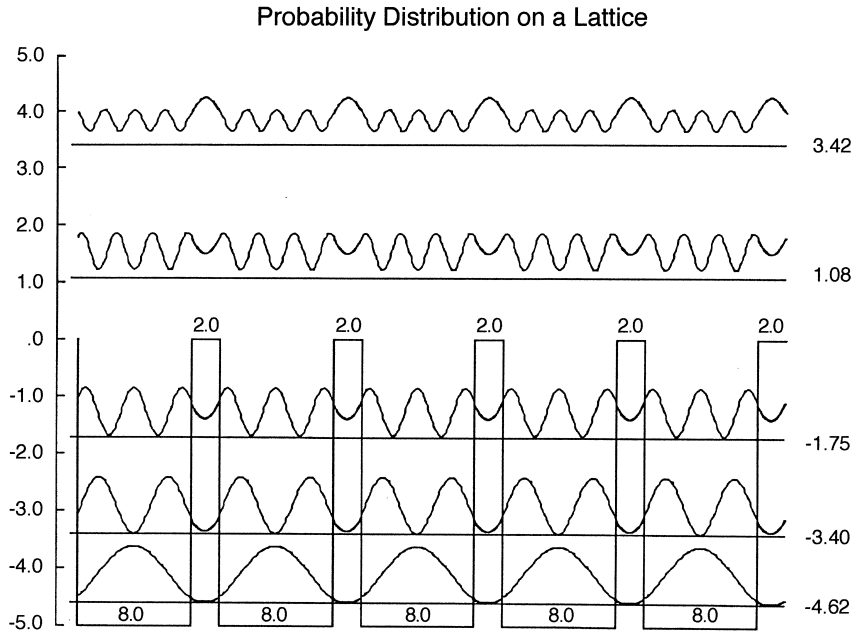


Fig. 42.2 Probability distributions for one eigenstate in each of the five lowest bands of the potential shown. The number of “nodes” increases with band number. It is clear that in an eigenstate, the probability distribution is the same in each cell of the lattice.

Remark: For $E < 0$ the bound state wavefunctions in Fig. 42.2 are real and exhibit nodes in the wells. The probability distribution goes to zero at the nodes. The lowest three states have zero-, one-, and two nodes. For $E > 0$ the wavefunctions do not have nodes (they are complex). The lowest two states with $E > 0$ have three- and

four “pseudo-nodes,” where the probability distribution has deep, nonzero minima in the wells.

43

Alloys

An alloy consists of a homogeneous mixture of two or more substances, usually metals. Energy bands can be computed for alloys just as they can be computed for pure substances.

In this chapter we will consider energy bands only for the simplest one-dimensional alloys. The alloys we consider are composed of equal numbers of two substances A and B in a periodic lattice of type $(AB)^N$. In Fig. 43.1 (top left) we show the potential for the unit cell of A , with $(V, \delta) = (-5.0, 8.0), (0.0, 2.0)$. The bound states for the corresponding single well potential are shown. They occur at ~ -4.6 , -3.4 , and -1.6 eV. To the right of this potential we show the density of states for the lattice A^N . The three bound states have been spread out into three bands. The density of states also shows a fourth band from ~ 0.2 to ~ 1.7 eV that arises from the first transmission resonance, and the lower part of a fifth band that arises from the second transmission resonance of the single well potential.

The potential for the unit cell of B ($(V, \delta) = (-2.0, 3.0), (0.0, 1.0)$) is shown on the second line of Fig. 43.1. The single bound state for the corresponding binding potential occurs just above -1.0 eV. To the right of this potential is the density of states plot for the periodic lattice B^N . The band arising from the single bound state extends from -1.6 to $+0.4$ eV. The upper levels in this band are unbound, even though the band arises from a bound state. The second band, extending above 1.2 eV, arises from the lowest transmission resonance.

The potential for the unit cell AB of the alloy with lattice $(AB)^N$ is shown on the bottom line of Fig. 43.1. The corresponding binding potential has four bound states. The two lower ones are essentially where they were in the pure A binding potential. The two upper levels have repelled each other slightly from their original positions

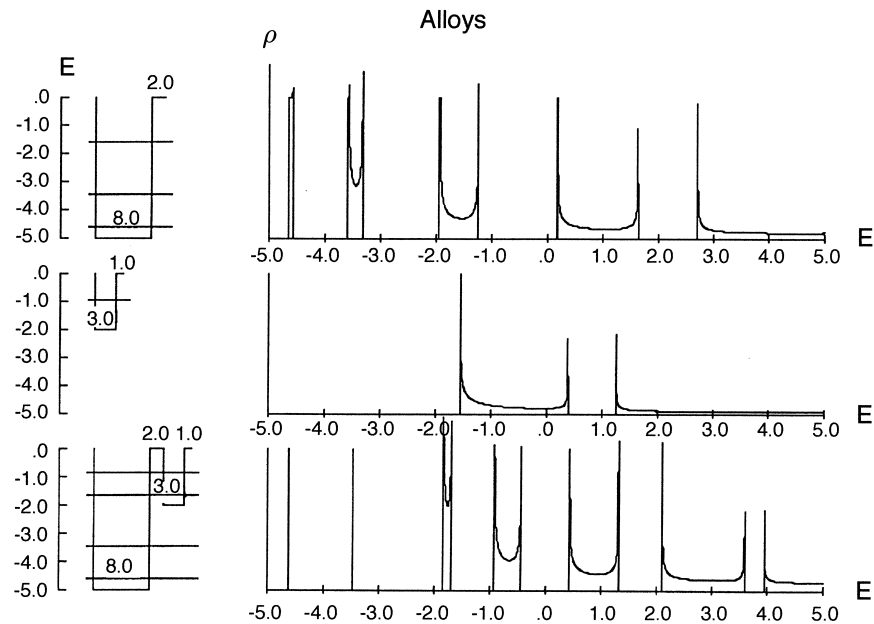


Fig. 43.1 *Top*, Potential A , eigenstates of corresponding single well potential, and density of states for corresponding periodic lattice A^N . *Middle*, Similar to top line, except for potential B . *Bottom*, Potentials A and B form the unit lattice potential AB . Eigenvalues and density of states for corresponding potential are shown.

in the A well and the B well. The third bound state is mostly confined to the A well and the fourth is mostly confined to the B well. This was determined by computing the eigenfunctions for the AB well.

The density of states for the periodic lattice $(AB)^N$ is shown to the right of the AB potential. The two lowest bands, derived from the A well, have been squeezed and are now so narrow that they cannot be resolved. These two bands have been squeezed because the classically forbidden region between adjacent A wells has been greatly increased by inserting the B potential. The third A band (-1.95 to -1.3 eV) has been squeezed to the region of ~ -1.8 eV, while the lowest B band (-1.6 to $+0.4$ eV) has been squeezed into (-0.9 to -0.5 eV), below the ionization threshold. The three bands that appear above 0.0 eV are not confined primarily to either the A well or the B well.

These results, and the conclusions drawn from them, are not strongly dependent on the actual shapes of the potentials. In Fig. 43.2 we repeat the calculations shown in Fig. 43.1 for smoother versions of potentials A and B . The potentials A and B of Fig. 43.1 have been replaced by smoother potentials with essentially the same bound

state spectra. The major differences are that the third band of the modified A potential extends above the ionization threshold while the first band of the modified B potential does not. The two lowest bands of the modified $(AB)^N$ potential are not as narrow as the corresponding bands in the original $(AB)^N$ potential (Fig. 43.1) because the classically forbidden region between two adjacent A wells is smaller. Otherwise, the density of states for the periodic potentials $(AB)^N$ in Fig. 43.1 and Fig. 43.2 are very similar.

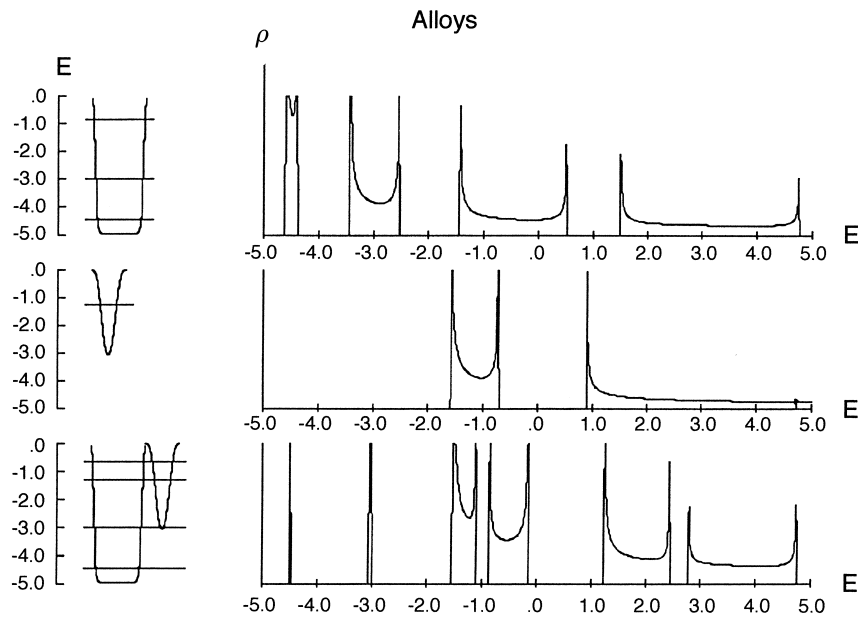


Fig. 43.2 Similar to Fig. 43.1 but with smoothed versions of potentials A and B , as shown. The modified potentials have bound state spectra similar to the unmodified potentials.

44

Superlattices

A one-to-one alloy containing unit cells of type A and B in a regular lattice has the one-dimensional spatial structure

$$\dots A B A B A B A B A B A B A B A B A B A B \dots \quad (44.1)$$

Imperfections in this regular structure often occur. They may take the form of inserting or deleting atoms of type A or B at various points in the lattice. In this chapter we consider imperfections that are caused by deleting atoms. The deletions involve alternating atoms of type A and B spaced at regular intervals. These deletions lead to regular lattices with a more complicated structure than the original lattice. For example, if every third atom is deleted from the regular lattice with unit cell (AB) ,

$$\dots A B \underline{A} B A \underline{B} A B \underline{A} B A \underline{B} A B \underline{A} B A \underline{B} A B \dots = [(AB)(BA)]^N, \quad (44.2)$$

we find a regular lattice with unit cell $[(AB)(BA)]$. A lattice of this type is called a *superlattice*.

Other superlattices can be obtained by deleting every fifth, seventh, \dots , $(2d+1)$ th atoms

d	$2d+1$	Regular Lattice	
1	3	$[(AB)^1(BA)^1]^{N/4}$	
2	5	$[(AB)^2(BA)^2]^{N/8}$	
3	7	$[(AB)^3(BA)^3]^{N/12}$	
d	$2d+1$	$[(AB)^d(BA)^d]^{N/4d}$	(44.3)

Each of the superlattices above has a total of N atoms, half of type A and half of type B . Since a superlattice obeys periodic boundary conditions, the allowed energy levels occur in bands. It may be expected that the band structure of a superlattice is closely related to the band structure of the parent lattice $(AB)^{N/2}$.

To explore this question, we can compute the band structure of a series of superlattices with increasing d . We choose unit cell parameters as follows

	A		B		
	V	δ	V	δ	
Region 1	0.0	1.0	0.0	0.5	(44.4)
Region 2	-5.0	8.0	-6.5	3.0	
Region 3	0.0	1.0	0.0	0.5	

In Fig. 44.1 we describe the changes that take place in a single band of the original $(AB)^{N/2}$ lattice when the alloy is converted to a superlattice with the same total number of atoms, as a function of increasing d . The $(AB)^{N/2}$ band that is presented in Fig. 44.1 extends from 3.5 to 4.6 eV. As usual, all bands behave in the same way, and this behavior is independent of the details of the potentials of A and B .

The regular lattice $(AB)^{N/2}$ has a band extending from 3.5 to 4.6 eV. For the superlattice with $d = 1$, the original band is split into two subbands. The two subbands are separated by a rather large band gap.

For the superlattice with $d = 2$, the original band has separated into four subbands. The two outer subbands are separated from the inner two by large band gaps. The inner two are separated by a very small gap at 4.1 eV.

In the superlattices with $d = 3, 4,$ and 5 , the original band has split into six, eight, and ten subbands. For $d = 3$ the six subbands are separated by three large and two small gaps at 3.8 and 4.45 eV. For $d = 4$ the eight subbands are separated by four large and three small gaps. For $d = 5$ there are five large and four small gaps.

In the case of the superlattice $[(AB)^d(BA)^d]^{N/4d}$, the original band has split into $2d$ subbands that are separated by $2d - 1$ band gaps, of which d are large and $d - 1$ are small. The large and small band gaps alternate with each other.

The structure of superlattice subbands can be viewed from a slightly different perspective. In going from the regular lattice $(AB)^{N/2}$ to the $d = 1$ superlattice $[(AB)^1(BA)^1]^{N/4}$ the original band splits into two subbands. In going from the $d = 1$ to the $d = 2$ superlattice, a new subband appears inserted between the two $d = 1$ subbands, squeezing these two outer subbands further past the band edges of the original $(AB)^{N/2}$ band. This new subband, extending from 3.8 to 4.5 eV, actually consists of two subbands separated by a narrow gap at ~ 4.1 eV.

In going from the $d = 2$ to the $d = 3$ superlattice, the narrow gap at ~ 4.1 between the two middle $d = 2$ subbands grows wider, extending from ~ 4.0 to 4.2 eV. Each of the two new well-separated subbands (3.7 to 4.0 eV and 4.2 to 4.7 eV) is split by a narrow gap (at 3.8 and 4.45 eV, respectively).

In progressing from the $d = 3$ to the $d = 4$ superlattice, a new band is inserted in the middle of the subband structure of the $d = 3$ superlattice. This new band extends from ~ 3.9 to 4.3 eV and actually consists of two subbands split by a narrow gap at ~ 4.1 eV.

The changes in the subband structure in going from the $d = 4$ to the $d = 5$ superlattice are similar to the changes that take place in going from the $d = 2$ to the $d = 3$ superlattice.

As Fig. 44.1 makes clear, it is useful to regard each band of the $(AB)^{N/2}$ lattice as breaking up into $d + 1$ “fat subbands” in the $[(AB)^d(BA)^d]^{N/4d}$ superlattice. The two outer fat subbands are not split while the inner $d - 1$ “fat subbands” each consist of two subbands separated by a narrow gap.

When the number of fat subbands is even ($d = 1, 3, 5, \dots$), a new fat subband is inserted right in the middle of the fat subbands in going from the d to the $d + 1$ superlattice. When the number of fat subbands is odd ($d = 2, 4, \dots$), then in going from the d to the $d + 1$ superlattice, the middle fat subband of the d superlattice “splits.” That is, the narrow band gap in that fat subband become large, and each of the two resulting subbands develops a narrow band gap.

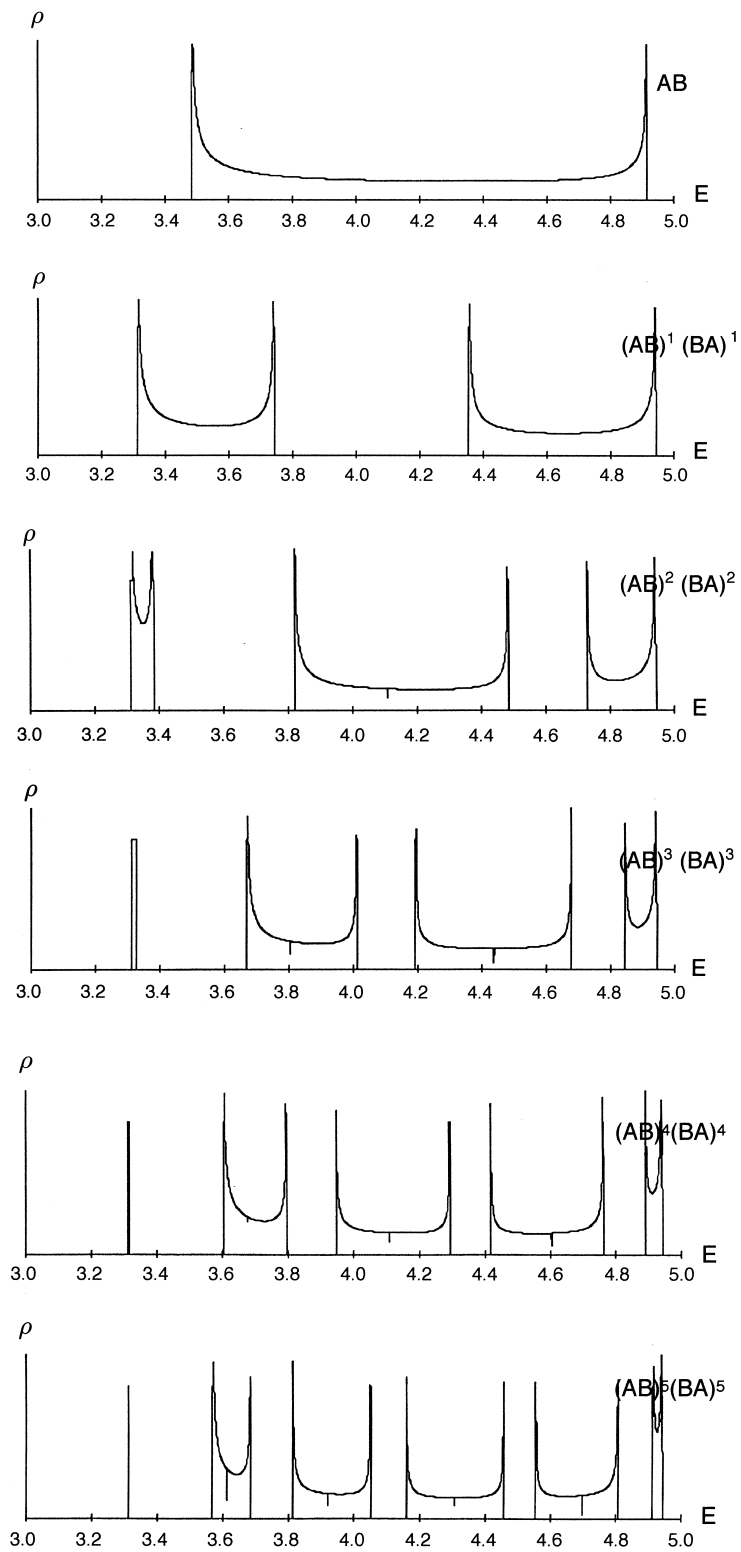


Fig. 44.1 Band structure of the $(AB)^{N/2}$ lattice, and the superlattices $[(AB)^d(BA)^d]^{N/4d}$ for $d = 1, 2, 3, 4, 5$.

45

Impurities

In the previous chapters we have seen how energy levels in periodic potentials of the type A^N occur in bands, with each band containing a total of N states. The same is true for regular alloys of type $(AB)^{N/2}$, as well as superlattices of type $[(AB)^d(BA)^d]^{N/(4d)}$.

It is difficult to grow crystal lattices of very high purity. Usually a crystal lattice contains impurities. We should therefore ask:

- Does the energy band structure of a pure lattice A^N persist in a lattice with impurities: $A^{N-1}B$?
- How are the electron wavefunctions affected by the presence of impurities?

These questions can be addressed relatively easily if we use what we have learned in previous chapters to simplify our computations as much as possible.

We exploit the following observations

- The band structure of a regular lattice A^N (N large) is apparent even for small values of N ($N \sim 5$).
- The band structure is unaffected by the type of boundary conditions imposed (bound state, scattering, periodic), for all practical purposes.

These observations suggest that we can determine the effects of impurities on the band structure and wavefunctions of a regular lattice by computing the band structure and wavefunctions for the bound states of a relatively small system $A^{N-1}B$, (N small).

To explore the effect of an impurity atom B on the properties of a regular lattice A^N , we have computed the bound state spectrum for two lattices of type A^3BA . The

results are shown in Fig. 45.1 and Fig. 45.2. In both figures the potential B depends on a parameter.

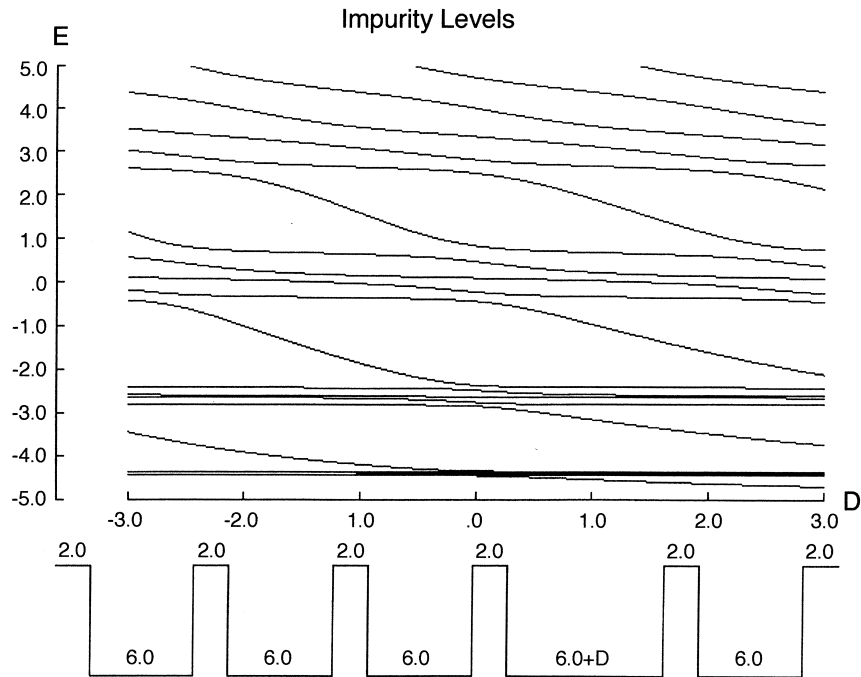


Fig. 45.1 Spectrum of bound state levels for the potential A^3BA as the width of the B impurity is varied. The A bands are represented by quartets of levels. Note that the eigenvalues do not cross. For this potential $V_L = V_R = 10.0$ eV.

In Fig. 45.1 both potentials A and B are 5.0 eV deep. The tops of the potentials are at 0.0 eV and the bottoms are at -5.0 eV. The width of potential A is 6.0 \AA while B has a width of $6.0+D \text{ \AA}$. The barriers separating wells are uniformly thick, at 2.0 \AA . The asymptotic potentials V_L and V_R are 10.0 eV to ensure that we see only bound states in the range scanned (-5.0 to $+5.0$ eV). For $D = 0$ the lattice is A^5 , and the bound state energies below 5.0 eV are gathered into four groups of quintets. We can easily see the effect that varying the width of B has on the energy-level structure. For D negative, the narrow B well has energies higher than the energies in a single A well. As D is increased, the lowest B level settles into the top of the lowest A band. The next B level, pressed up against the bottom of the third A band, peels off and settles onto the top of the second A band. The next higher B level behaves similarly. For $D > 0$, the B well is wider than the A well and its spectrum has lower-lying levels. This behavior is reflected in Fig. 45.1. As D increases through

0.0 Å, the lowest-lying level in each band falls away from the bottom of the band and approaches the top of the next lower A band. Of course, the lowest B level has no lower A band to settle onto.

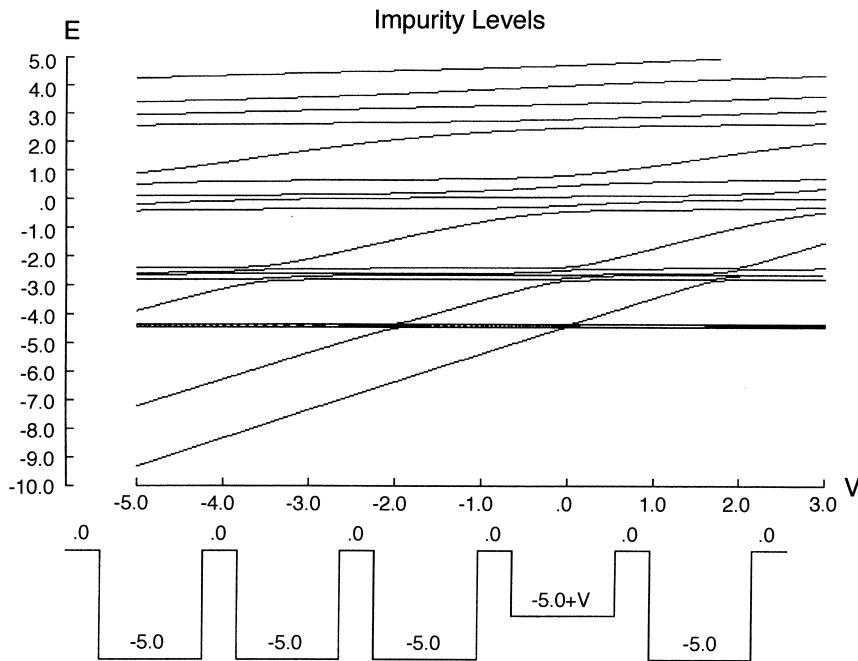


Fig. 45.2 Spectrum of bound state levels for the potential A^3BA as the depth of the B impurity is varied. The A bands are represented by quartets of levels. Note the the eigenvalues do not cross. For this potential $V_L = V_R = 10.0$ eV.

Fig. 45.2 tells a similar story. Here the wells all have the same width (6.0 Å). The barriers at 0.0 eV have width 2.0 Å. Each A well is 5.0 eV deep, while the bottom of the B well is at $-5.0 + V$ eV. The B well is varied in depth from -10.0 eV ($V = -5.0$ eV) to -2.0 eV ($V = +3.0$ eV). Once again, the band structure of A^N is represented by four groups of quintets for A^5 at $V = 0.0$ eV. As the bottom of the B well is increased from -10.0 eV to -2.0 eV, the bound state energies due to B increase almost linearly (with a slope of $+1$). However, the B levels do not cross the A bands. Rather, a B level approaches the bottom of an A band, and then, at a slightly greater value of V , the highest level in the A band peels off and rises linearly with increasing V until it runs into the bottom of the next higher A band.

These two figures make it clear that, in some sense, there is a “conservation of number of levels” in going from a regular lattice A^N to a lattice with impurity $A^{N-1}B$ (or some cyclic permutation). The band structure is not lost, merely perturbed. Bands

with N levels in A^N are replaced by bands with $N - 1$ levels in $A^{N-1}B$, and additional B levels are scattered in appropriate places in the energy-level spectrum.

The energy eigenfunctions are perturbed as follows. For eigenvalues in a band of levels, the corresponding wavefunctions extend over all the A atoms. For any eigenstate in an A band, the probability distribution is essentially the same in every cell of type A , except possibly in the A cells adjacent to the B impurity. However, the nondegenerate states between A bands have wavefunctions that are largely localized to the B atom impurity.

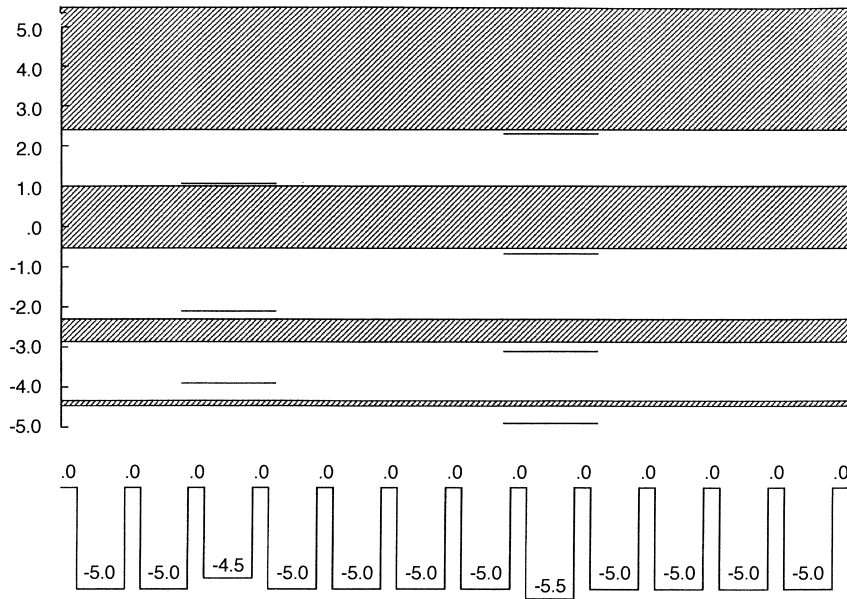


Fig. 45.3 Bands and impurity levels in a lattice of type $A^{n_1}BA^{n_2}B'A^{n_3}$. The bands are shown extending over the entire lattice. The donor level, over B' with depth 5.5 eV, lies slightly below the lowest unfilled or partly filled A band. The acceptor level, over B with depth 4.5 eV, lies slightly above the highest filled or almost filled A band.

In Fig. 45.3 we show a lattice $A^{n_1}BA^{n_2}B'A^{n_3}$. The A levels occur in the bands indicated. Since the A -like eigenstates extend over the entire lattice, the bands are shown extending over the lattice. The B level at -4.5 eV provides three levels that occur above the A bands. Since the wavefunctions, with $n = 0, 1, 2$ nodes, are largely confined to this well, the energy level is shown extending over only this well and its adjacent barriers. The B' level at -5.5 eV provides four levels that occur beneath the A bands. Since the wavefunctions, with $n = 0, 1, 2, 3$ nodes, are largely confined to this well, the energy level is shown extending over this B' well and its adjacent barriers.

Impurity levels that occur below an energy band that contains few or no electrons are called donor levels. If these impurity levels contain an electron, that electron is “stuck” to the impurity site. However, that electron can be promoted (donated) into the empty band just above the donor level at relatively low energy cost. In the empty band, the electron is mobile: it can move relatively freely from A atom to A atom. The level of the B' well (with depth 5.5 eV) just below the lowest empty A band is a donor level.

An empty impurity level just above a filled A band is called an acceptor level. At relatively low energy cost, this level can remove (accept) an electron from the filled band just below it. This leaves a “hole” in the filled band. This hole acts in many ways like an electron of opposite charge. The level of the B well (with depth 4.5 eV) just above the highest-filled A band is an acceptor level.

Careful control of the concentrations and types (donor, acceptor) of dopants in semiconductors have been responsible in large part for the current computer revolution.

46

Quantum Engineering

The availability of energy resources will be one of the major points of political friction in the twenty-first century.

46.1 ENERGY SOURCES

The energy resources that currently contribute more than an infinitesimal fraction of the world's energy needs are listed in Table 46.1.

Coal, oil, and gas are the major sources of energy in today's economy. They are "nonrenewable" and are currently being rapidly depleted. We believe these energy sources are of fossil origin. This means that the energy stored in these resources derives ultimately from the transformation of solar energy to biomass, at very low efficiency, followed by death, sedimentation, conversion, and storage (also at very low efficiency) over a very long period of time. These resources have been created by natural processes that continue to this day. The time scale for creation of these resources is millions of years; the time scale for depletion is hundreds of years. Therefore, although these resources are in principle renewable, they are in practice nonrenewable unless we learn how to accelerate the creation process by factors in excess of 10^4 . Burning these fossil fuels releases large amounts of CO_2 and other pollutants into the atmosphere.¹ It is widely believed that this has a negative environmental impact. In addition, it destroys a reservoir of raw materials for industry.

¹M. I. Hoffeert et al., Advanced Technology Paths to Global Climate Stability: Energy for a Greenhouse Planet, *Science* 298 (2002): 981-87.

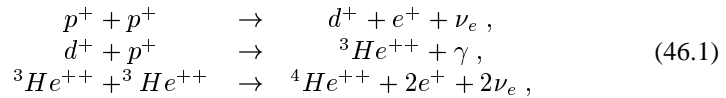
Table 46.1 Energy resources

Energy Source	Comment
Coal	“Nonrenewable”
Oil	
Gas	
Fission	Radioactive
Fusion	
Geothermal	
Tidal	Gravitational
Hydroelectric	Gravitational/solar
Wind	Solar
Biomass	
Solar	

Some people regard this loss as even more severe than possible negative impact on our atmosphere.

The next three energy sources listed in Table 46.1 involve nuclear transformations. Nuclear fission (“splitting”) involves splitting heavy nuclei into lighter nuclei, releasing energy. This process, initially demonstrated on the earth in atomic bomb explosions, has successfully been tamed. It is now the basis of energy production in nuclear power plants that generate a substantial fraction of electrical energy in the industrial nations of the earth. When not handled carefully, nuclear accidents can occur (Three Mile Island, Chernobyl, . . .). The worst accidents have led to environmental catastrophes. That is, large areas are rendered uninhabitable for long periods by high levels of radiation. Although the radioactivity levels gradually die away (along with the population), the half-life for decay is comparable to or longer than the human time scale (~ 70 years). This renders fission a problematic energy source for the future.

Nuclear fusion involves combining lighter elements to form heavier elements, releasing energy in the process. Fusion of hydrogen to helium,



is the principle fusion process that powers our star, the sun. This process was demonstrated on the earth with the explosion of the first hydrogen bomb. Since then, it has been a goal to tame this reaction and allow it to run in a controlled, continuous way in order to generate energy for the world’s needs. An enormous amount of time, money, and intellectual energy has been devoted to this goal. Estimates of the amount of time

and money required to reach a commercially viable result have diverged rather than converged—the end is nowhere in sight and receding further from reach all the time.

Geothermal energy is a natural resource that is derived in second order from nuclear fission. Long-lived radioactive isotopes within the core and mantle of the earth decay, releasing energy that heats up the surroundings. The hot plastic material of the core and mantle flows with a geological time scale. This material comes close to the surface at some parts of the earth's surface, principally at boundaries between the earth's plates. The temperature difference between the hot interior magma and the cooler fluids on the earth's surface can be used in the usual way to generate heat and electrical energy. Although this resource is nonrenewable, its time scale is so long that, for all practical purposes, it can be considered as permanent.

The motion of the earth and moon about their center of mass, and of the earth-moon system about the sun, raises diurnal tides on the surface of the earth. The differing physical properties of the material on the earth's surface (water, rock) allows us to create differences in gravitational potential energy that ultimately can be transformed to electrical energy. Tidal energy will never provide more than a small percentage of the earth's energy needs. It is essentially perpetual and nonpolluting. However, it does require modification of parts of the earth's surface and in that sense does have a nontrivial environmental impact.

Hydroelectric energy is derived from the conversion of the energy in falling water into electrical energy. Water is raised from sea level by evaporation (solar energy) and deposited at higher altitudes by precipitation as rain or snow. At higher elevations it possesses gravitational potential energy. Since this energy conversion process occurs naturally,

All the rivers run into the sea;
 Yet the sea is not full;
 Unto the place from whence the rivers come,
 Thither they return again. Ecclesiastes 1:7

Hydroelectric conversion is nonpolluting. It is also 'perpetual,' or at any rate will last as long as there is water on the surface of the earth. However, it also involves modifying selected parts of the earth's surface, so in this sense it also has nontrivial environmental impact.

Wind motion and biomass conversion are energy sources that originate almost entirely with the conversion of incident solar radiation. Since they are also naturally occurring processes, they are renewable and nonpolluting. However, they also involve modification of the environment, so to some extent are subject to political and environmental constraints.

Tidal, hydroelectric, and wind power sources will not provide more than a small percentage of the earth's energy requirements. Biomass conversion has the potential to make a more substantial contribution, although it is not likely to.

The sun is ultimately the source of all but the radioactive energy sources. Solar energy can be converted directly to industrially useful energy in two ways (neglecting conversion to biomass):

1. directly to heat
2. directly to electrical energy.

In the former case, a large number of concentrating mirrors, spread over an area the size of one or more soccer fields, are used to focus sunlight into a very small volume. Within this volume the temperature can reach 5000 K. Such solar furnaces can be used to drive electrical turbines or used as research facilities. More mundane but commercially much more important applications involve absorbing sunlight to produce hot (80°C) water rather than wasting electricity to heat water.

Sunlight can be transformed directly to electrical energy by being absorbed in crystals that are designed to allow the absorbed energy to separate positive from negative charges. Solar panels composed of such crystals are routinely used in the space program. They are also used, with increasing frequency as costs drop in places where cost or maintenance is more of a problem for other types of energy sources.

We will describe how to design crystals for direct solar conversion later in this chapter.

46.2 ENERGY CONSUMPTION

The total energy that has been consumed by the earth's population in the year 2000 has been estimated to be about 500 exajoules (500×10^{18} J). It is convenient to convert this energy consumption per year into power measured in Watts (joules/sec). This is done by dividing by the number of seconds in a year. This is 3.15×10^7 sec (mnemonic: $\pi \times 10^7$ sec). The rate of energy consumption in 2000 is then about 1.58×10^{13} W.

We compare this energy consumption rate with the rate at which solar radiation energy is incident at the top of the earth's atmosphere. This number, the "solar constant," is 1368 W/m^2 according to earth satellite measurements.² This number is not actually constant: it varies primarily because of small variations in solar energy output (fluctuations of order 0.01%, or one part in 10^4 , are observed) and variation in the earth-sun distance due to the eccentricity of the earth's orbit. For this reason, we will refer to this measured value as the "solar irradiance." The total power received by the earth at its mean solar distance is

$$P = 1368 \text{ W/m}^2 \times \pi (6370 \text{ km})^2 = 1.74 \times 10^{17} \text{ W}, \quad (46.2)$$

where the earth's radius is approximately 6370 km. About $\frac{3}{4}$ of this energy filters down to the surface of the earth as radiation in the visible part of the spectrum.

It is instructive to compare the rate at which energy is consumed by the world's population to the rate at which radiant energy is received from the sun by the earth. This ratio is

²K. J. H. Phillips, *Guide to the Sun*, Cambridge, UK: Cambridge University Press, 1992.

$$R = \frac{\text{Power consumed}}{\text{Power received}} = \frac{1.58 \times 10^{13} \text{W}}{1.74 \times 10^{17} \text{W}} \sim 10^{-4}. \quad (46.3)$$

That is, mankind's energy consumption is comparable to fluctuations in the sun's energy output or, more accurately, the solar irradiance (i.e., including changes due to the earth's orbital parameters). So if we believe, as some do, that changes in insolation (solar radiation received by the earth) due to changes in the earth's orbital parameters are responsible for the ice ages that the earth has experienced over the last several million years, then it is just a short additional step to believe that twentieth-century industry's contribution to the earth's energy budget could also be responsible for dramatic earth climate changes.

Direct conversion of solar radiation to electrical energy has two benefits that are worth mentioning explicitly.

1. The fusion process ($4p^+ \rightarrow {}^4\text{He}^{++} + 2e^+ + 2\nu_e + 2\gamma$) that liberates energy also produces radioactivity in the surrounding environment. If we were able to control fusion on the earth's surface, we would still face the problem of caring for the nearby material made radioactive by this process. As it is, any radioactivity produced is produced in the sun. We do not have to worry about it.
2. Direct conversion of sunlight to electrical energy is a "neutral" process. It neither adds to nor subtracts energy from the earth's natural budget (in first order). At most, it redistributes energy from one geographical location to another. Because of this redistribution, there may be a second-order effect on the earth's energy budget. In short, this process is nonpolluting but could have local environmental impacts.

46.3 SIMPLE SOLAR CELLS

The spectrum of visible (to humans) solar radiation extends from the violet (400 nm or 4000 Å) to the red (700 nm or 7000 Å). The peak intensity is in the yellow at about 580 nm or 5800 Å. The sun behaves to a reasonable approximation as a blackbody with a temperature about 5778 K. (This blackbody looks yellow!)

Radiation in the violet at a wavelength of 400 nm consists of photons, each carrying an energy of about 3.1 eV. Similarly, "red photons" at 700 nm have an energy of 1.8 eV. Yellow photons carry 2.1 eV. We therefore expect solid-state devices that are designed to absorb solar radiation and convert it into electrical energy to have band gaps in the range of 1 to 3 eV.

A relatively simple solar conversion device is shown in Fig. 46.1. In this device two layers of impurity-doped silicon are placed over a glass substrate. One layer is doped with electron donors (*n* type), the other is doped with electron acceptors (*p* type). Both layers are bound to conducting metal contacts (the external leads, or wires). An antireflection coating is applied to the top of the cell to reduce losses

of incident solar radiation by suppressing reflection. The glass substrate is usually designed to be reflective. This reflects unabsorbed solar radiation back through the cell, so the cell is effectively “twice as thick.”

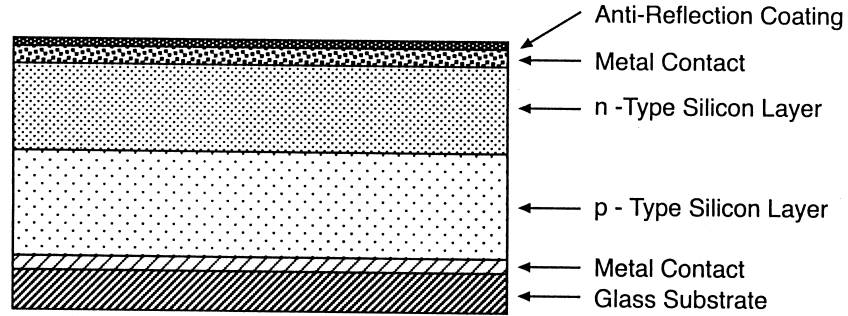


Fig. 46.1 Simple solar cell. *n*- and *p*-doped silicon layers are sandwiched between metallic contacts. The top of the cell is coated with an antireflection coating, and the glass substrate is usually reflective. Incident light creates an electron-hole pair. The electron is attracted to the *n*-type silicon layer, the hole is attracted to the *p*-type silicon layer.

The energy band structure for this device is shown schematically in Fig. 46.2. Two energy bands are shown. At zero temperature the lower (valence) band is filled and the upper (conduction) band is empty. At finite temperature some electrons are excited from the valence band to the conduction band. The probability that a state with energy E is filled is given by the Fermi-Dirac function

$$FD(E, T) = \frac{1}{e^{(E-\mu)/kT} + 1}. \quad (46.4)$$

Here T is the temperature, measured in kelvins, k is Boltzmann's constant, $k = 1.38 \times 10^{-16}$ erg/K = 8.616×10^{-5} eV/K, kT is an energy, and μ is a chemical potential. At room temperature ($T = 300$ K) $kT = 0.0258 \sim \frac{1}{40}$ eV.

Under equilibrium conditions, the probability that an electron is in any state in the conduction or valence band is determined by a single chemical potential. However, the absorption problem is not an equilibrium problem. Rather, it is a dynamic process for which we seek a steady state solution. Under this condition the probability distribution for electrons in the valence band is determined by one chemical potential, μ_V , while that for the conduction band is determined by another chemical potential, μ_C :

$$FD_{VB}(E, T) = \frac{1}{e^{(E-\mu_V)/kT} + 1}, \quad (46.5)$$

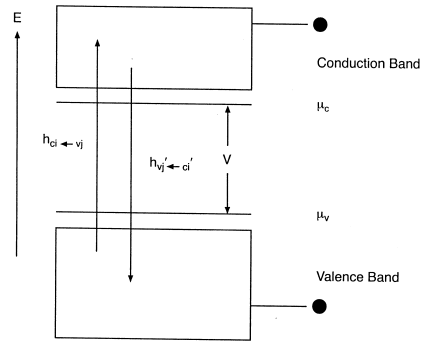


Fig. 46.2 Energy band diagram for a simple solar cell operating with two active bands, a conduction band and a valence band. The chemical potentials μ_C and μ_V , defining the nonequilibrium steady state populations in the two bands are shown.

$$FD_{CB}(E, T) = \frac{1}{e^{(E - \mu_C)/kT} + 1}. \quad (46.6)$$

The potential difference, V , at which the cell operates, is determined by

$$qV = \mu_C - \mu_V. \quad (46.7)$$

We now define $n(\nu, z)$ to be the number of photons of frequency ν that occur a distance z inside the cell ($z = 0$: front surface; $z = 1$: back surface). This number changes as we progress through the crystal for two reasons:

1. Photons of frequency ν are absorbed.
2. Photons of frequency ν are reemitted.

In the absorption process, an electron is removed from state j in the valence band and deposited in state i in the conduction band. The rate at which this happens is proportional to

1. the probability that state V_j is occupied: $FD_{V_j}(E, T)$
2. the probability that state C_i is not occupied: $1 - FD_{C_i}(E, T)$
3. a transition matrix element: $H_{C_i \leftarrow V_j}$
4. the number of photons: $n(\nu, z)$
5. the factor n/c , $n =$ index of refraction.

$$\text{Absorption : } \quad \frac{dn(\nu, z)}{dz} = -\frac{n}{c} \sum_{i,j} H_{C_i \leftarrow V_j} n(\nu, z) F D_{V_j} (1 - F D_{C_i}) . \quad (46.8)$$

Photons are also reemitted into the field according to

$$\text{Emission : } \quad \frac{dn(\nu, z)}{dz} = +\frac{n}{c} \sum_{i,j} H_{V_j \leftarrow C_i} [n(\nu, z) + 1] F D_{C_i} (1 - F D_{V_j}) . \quad (46.9)$$

The emission contribution comes from two processes: stimulated emission (proportional to $n(\nu, z)$), the process responsible for laser action; and spontaneous emission (proportional to 1 within the square brackets). The matrix elements for the absorption and emission processes are complex conjugates of each other: $H_{C_i \leftarrow V_j} = H_{V_j \leftarrow C_i}^*$.

By integrating these equations through the crystal, from the front to the back, and then back to the front again, and imposing suitable boundary conditions, it is possible to compute qV (the energy delivered), the power output, and the operating efficiency of the solar cell, as a function of the band gap. This was done by Shockley and Queisser in 1961.³ The result is that at room temperature, the theoretical maximum conversion efficiency is 40.7%. This occurs with a band gap of 1.1 eV.

Increasing the efficiency of a solar cell means that a smaller geographic area is required to produce an equivalent amount of electrical energy. To be explicit, the world's energy could be supplied by about 130,000 km² solar cells on the earth surface operating at 50% efficiency. By increasing the conversion efficiency by 1% we could produce the same energy with about 3000 km² smaller area.

Luque and Martí⁴ have explored the possibility of increasing the conversion efficiency of a solar cell by inserting an impurity band between the valence and conduction bands (Fig. 46.3). They set up equations describing absorption and reemission of photons between all three pairs of bands and explored the energy band parameters that maximized the conversion efficiency of incident solar radiation to output electrical energy. In this configuration, the maximum theoretical conversion efficiency is 63.1%. This occurs when the band gap between the valence and conduction bands is 1.93 eV and the impurity band is 0.7 eV above the top of the valence band.

46.4 THE DESIGN PROBLEM

We now describe how to design a quantum mechanical device that approximately meets these specifications.

³W. Shockley and H. J. Queisser, *Journal of Applied Physics* 32 (1961): 510-5??.

⁴A. Luque and A. Martí, Increasing the Efficiency of Ideal Solar Cells by Photon Induced Transitions at Intermediate Levels, *Physical Review Letters* 78 (1997): 5014-5017.

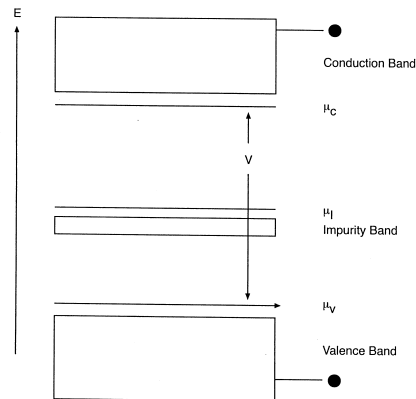


Fig. 46.3 Energy band diagram for a solar cell operating with three active bands: a conduction band, a valence band, and an impurity band between the two. The chemical potentials defining the nonequilibrium steady state populations in the three bands, μ_C , μ_I , and μ_V , are shown.

The steps involved in designing a device meeting the specifications just proposed—a gap of 1.93 eV between the valence band and the conduction band and an impurity band 0.7 eV above the valence band—are relatively simple. As a first step, we look for an “atom” whose lowest unoccupied state is more than 1.93 eV above the highest occupied state. When many atoms of this type are brought together into a regular lattice, the bound states are spread out into bands, and the energy between the top of the highest occupied (valence) band and the bottom of the lowest unoccupied or unfilled (conduction) band is reduced. For such substances, we compute the band structure. Those atoms (“*A*” atoms) for which the band gap is near 1.93 eV are of interest. We then search for atoms (“*B*” atoms) for which there is an unoccupied orbital 0.7 eV above the top of the valence band. This orbital need not be the lowest empty orbital. Such atoms can serve as impurity atoms. When a lattice of *A* atoms is doped with *B* atoms, an impurity band will be produced between the *A*-type valence and conduction bands. If the doping percentage is small, the impurity band will be very narrow and the locations of the *A*-atom valence and conduction bands will be essentially unaffected.

To illustrate this process, we consider an *A* “atom” represented by a well of depth 7.0 eV and width 8.0 Å. Such atoms have four bound states at $E = -6.58, -5.35, -3.37,$ and -0.87 eV, where we have chosen the potential at $\pm\infty$ to be 0.0 eV. If the lowest three levels are occupied, then the energy gap between the highest occupied level at -3.37 eV and the lowest unoccupied level at -0.87 eV is 2.5 eV. If the unit cell for the *A* atom in a lattice is described by potentials and widths as shown in Table 46.2, then each of the four levels is broadened into a band, as shown in Table 46.3.

Table 46.2 Parameters for potentials of type *A* and *B*

A		B	
V (eV)	$\delta(\text{\AA})$	V (eV)	$\delta(\text{\AA})$
0.0	1.0	0.0	1.0
-7.0	8.0	-4.8	6.0
0.0	1.0	0.0	1.0

Table 46.3 Bound states and bands for atoms of type *A*

Level Number	Single Particle Energy	Top of Band Bottom of Band	Band Width	Band Gap
4	-0.87	-0.16	1.03	1.93
		-1.19		
3	-3.37	-3.12	0.45	1.68
		-3.57		
2	-5.35	-5.25	0.17	1.14
		-5.42		
1	-6.58	-6.56	0.04	
		-6.60		

This table shows that the gap between the third (valence) and the fourth (conduction) band is 1.93 eV.

With *A* as host atom, an atom of type *B* should have an unoccupied level at $-3.12 + 0.70 = -2.42$ eV. The potential *B* shown in Table 46.2 has bound states at $E = -4.19, -2.44,$ and -0.14 eV. If the second level at -2.44 eV is unoccupied, *B* atoms will serve as impurity atoms in a lattice of *A*-type atoms to achieve the desired specifications. In Fig. 46.4 we show part of a one-dimensional lattice of *A*-type atoms with a single impurity atom of type *B*. Above this potential we show the four bands

that arise from the four levels that the potential A possesses, as well as the three levels (dashed lines) provided by B atoms. As long as the doping level is small (few percent or less) the location of the bands and impurity levels is unaffected by the doping level—it is only the number of impurity states that changes with the doping density.

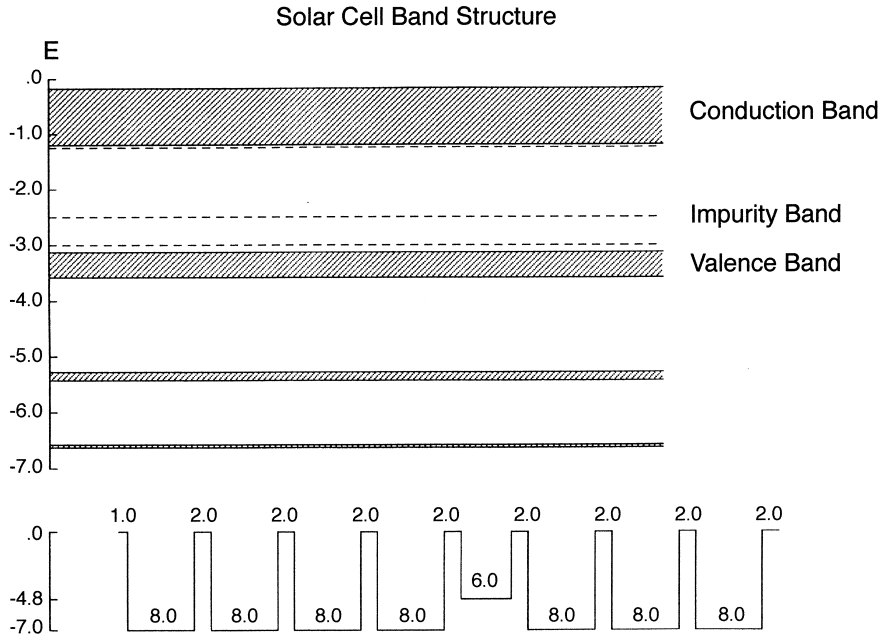


Fig. 46.4 A lattice of A atoms with a low density of B atoms produces a band structure as shown. Chemical potentials for the three bands are indicated by dashed lines. The potential parameters for the two “atoms” are presented in Table 46.2. This impurity-doped lattice meets the design criteria for a solar cell with maximum possible efficiency under the conditions stated.

In the real world we cannot design atomic potentials: we are stuck with what nature gives us. However, in the real world the basic ideas for designing devices are not much different from those described above.

Index

- Absorption process, 217
- Acceptor levels, 208–209
- Action, 54, 78, 115–116, 161
 - integral, 97
- Adjacent wells, 127
- Algorithm, 93
 - computational, 16
- Alloys, 197–199
- Amplitude
 - probability, 20, 28
- Analytic continuation, 115
- Ansatz, 159
- Antireflection coating, 216
- Artifacts, 46
- Association of states, 125
- Asymptotic, 47
 - behavior, 181
- Avoided crossings, 117–119
- Backscattering, 182
- Band, 113, 153, 205
 - active, 216
 - conduction, 216, 218
 - edges, 173, 181, 202
 - gap, 181
 - of allowed energies, 173
 - of allowed states, 179
 - of resonances, 197
 - of wavefunctions, 192
 - splitting of, 202
 - structure, 205
 - structure - for solar cell, 221
 - structure - for superlattice, 201–202
 - valence, 216, 218
- Barriers
 - attracting, 40, 42, 54
 - combining, 71
 - double, 57
 - multiple, 65
 - quadruple, 65
 - rectangular, 37
 - repelling, 55
 - shape of, 43
 - triple, 65, 71
- Behavior
 - asymptotic, 47
- Best approximation, 130
- Best fit, 128
- Bias, 80
- Bifurcations, 104–105
- Bifurcation
 - saddle-node, 118
- Binding
 - boundary conditions, 165
- Blackbody, 215
- Bohr quantization condition, 96
- Boltzmann's constant, 216
- Boundary, 7
 - and wavefunctions across, 7
- Boundary conditions, 27, 35, 82, 165
 - and energies, 188

- for bound states, 165
- for periodic potentials, 30, 165
- for scattering, 165
- matching, 7
- periodic, 30
- relations among, 185
- Bound states, 89, 103, 112, 188
 - and scattering resonances, 141
 - annihilation of, 145
 - avoided crossings, 117, 119
 - boundary condition for, 28
 - creation of, 49, 107, 145
 - energies of, 143
 - relation with scattering states, 103
 - relation with transmission resonances, 141
 - wavefunctions, 121
- Bowling ball, 39
- Bragg scattering condition, 182
- Building blocks, 81
- Center of gravity, 65
- Charge, 31
- Chemical potential, 216, 218, 221
- Classical action, 54
- Classical mechanics, 38
- Coding, 41, 93, 177
- Comparisons
 - qualitative, 127
 - quantitative, 127
- Computational algorithm, 16
- Conduction band, 216, 218
- Conservation
 - of momentum, 21
 - of number of levels, 208
- Continuum
 - ripple in, 147
- Conversion efficiency, 218
- Creation
 - of bound states, 107
- Crystal, 165
- Deep resonance, 63
- Degeneracy, 156
- Degenerate eigenvalues, 133
- Delocalized, 124, 126
- Density of states, 173, 177, 197
- Dependence
 - on parameters, 99
- Design specification, 77
- Determinant, 20, 167
- Device, 77
- Diagonalize
 - transfer matrix, 167
- Digestion
 - of resonance, 148
- Donor levels, 208–209
- Dopants, 209
- Dope, 149
- Doping percentage, 219
- Double barrier, 57
- Doublet, 65, 70, 111–112, 115, 133
- Double-well potential, 111
- Double well potential, 112, 115, 117
- Duality, 20
- Edges
 - of bands, 202
- Eigenfunctions, 121
- Eigenvalue equation, 4
- Eigenvalues
 - avoided crossings, 119
 - degenerate, 133
 - scattering of, 168
 - unit circle, 168
- Electron, 31, 80
 - donor, 215
 - gun, 35
 - volt, 31
- Emission
 - process, 218
 - spontaneous, 218
 - stimulated, 218
- Energies and boundary conditions, 188
- Energy
 - band, 149, 153, 173, 177, 179, 192, 197, 218
 - band plot, 173
 - eigenfunctions, 208
 - gap, 219
 - level diagram, 173
 - reduced, 94
- Energy resources, 211
 - biomass, 211
 - geothermal, 213
 - hydroelectric, 213
 - nonrenewable, 211
 - renewable, 211
 - solar, 214
 - tides, 213
 - wind, 213
- Energy
 - thermal, 80
- Even parity, 133
- Even wavefunctions, 123
- Exajoule, 214
- Expansion coefficients, 132
- Fat subband, 203
- Fermi-Dirac function, 216
- Filter, 77
- Fingerprints, 73
- Forbidden region, 39
- Four well potential, 112–113, 138–139
- Free particle, 181–182
- Fusion of nuclei, 212
- Gaussian
 - potential, 53, 122, 161

- potential - attracting, 45
- potential - repelling, 44
- shape, 43
- Geothermal
 - energy resources, 213
- Ground state, 134
- Half width, 105, 119
- Hamiltonian, 1
 - mechanics, 158
- Hole, 209
- Hydrogen atom, 32
- Hyperbolic functions, 121
- Imperfections, 201
- Impurities, 205
- Impurity
 - acceptor levels, 208–209
 - band, 208, 219
 - donor levels, 208–209
 - doped lattice, 221
 - doping, 150
 - doping - of silicon, 215
 - eigenfunctions, 208
 - levels, 151, 206–207
- Index of refraction, 217
- Inner product, 128
- Insulation, 215
- Interference effects, 154
- Interior region, 16
- Interleaving, 188
 - of binding state eigenvalues, 186
 - of bound state eigenvalues, 185, 188
 - of periodic states, 185–188
 - of resonance peaks, 185–186, 188
- Intermediate symmetry, 138
- Ionization threshold, 112–113, 124, 198
- Isolated state, 112
- Kinetic energy, 4
- Lagrangian mechanics, 158
- Laser, 218
- Lattice, 165, 205, 208
 - band structure of, 201
 - probability distribution for, 195
- Leakage
 - into adjacent wells, 156
- Least squares, 130
- Length scale, 32
- Level splitting, 115, 117
 - logarithm of, 115
- Linear combinations
 - symmetrized, 136
- Linear superposition, 128
- Line shape, 62
 - Gaussian, 62
 - Lorentzian, 58, 62
- Localization
 - of wavefunction, 150
- Lorentzian
 - line shape, 58
 - peaks, 104
- Matching
 - of wavefunctions, 10
- Matrix
 - scattering, 20
 - transfer, 13–15
- Maxima, 70
- Momentum, 4
 - conservation of, 21, 23, 35
 - operator, 4
- Multiple
 - barrier potential, 111
 - barriers, 65
- Multiplet, 77–78
- Multiple
 - well potential, 111, 113, 154
- Node
 - forcing of, 135
- Nodes, 122, 134
- Normalize, 122
- N -tuple, 65, 113, 149
 - of transmission resonances, 113
 - width of, 186
- n type dopant, 215–216
- Nuclear
 - fission, 212
 - fusion, 212
 - transformations, 212
- Odd
 - parity, 133
 - wavefunctions, 123
- One-dimensional array, 165
- Ordinary differential equations, 158
- Overlap
 - integral, 128, 131–132
 - integrals, 127
 - matrix, 130
- Overlapping peaks, 105
- Parameter
 - splitting dependence on, 117
- Parentage, 149
 - of wavefunctions, 133, 156
- Parent lattice, 202
- Parity, 133
 - alternation of, 134
 - of eigenstates, 135
- Particular solutions, 9
- Pass band, 80
- Peaks
 - Lorentzian, 104
 - overlapping, 105
 - unresolvable, 82
- Periodic
 - boundary conditions, 30, 165

- lattice, 177
- potential, 172, 188, 192
- Phase angles
 - allowed, 173
- Phase shift, 51, 54
 - for unit cell, 193
 - measurement, 89
 - reflection, 78
 - total, 96
- Planck's constant, 1
- Potential
 - attracting barrier, 46
 - attractive, 95
 - difference, 80
 - double well, 111, 115
 - four well, 112–113
 - multiple well, 111, 113
 - multiwell, 154
 - piecewise constant, 13, 15
 - scattering, 20
 - shape of, 95
 - three well, 112–113
- Probability
 - amplitude, 20, 23, 28, 35, 122
 - density, 122
 - distribution, 67, 70, 136, 191, 194
 - distribution for symmetric states, 135
 - distribution in a lattice, 195
 - distributions for antisymmetric states, 135
 - distributions in a lattice, 195
 - invariance of in a lattice, 195
 - reflection, 28
 - transmission, 28
- Proton, 32
- Prüfer transform, 157, 159
- Pseudo-nodes, 196
- p* type dopant, 215–216
- Qualitative, 127
- Quantitative, 127
- Quantization condition, 167–168
 - Bohr, 96
- Quantum engineering, 77, 149, 211
- Rectangular barrier, 37
- Reduced energy, 94
- Reflection
 - of particle, 35
 - phase shift, 78
 - probability, 28, 36
 - suppression of, 216
 - symmetry, 123
- Region
 - interior, 16
- Repelling
 - barrier, 38, 55
 - Gaussian potential, 44
- Resolution, 57, 81
- Resolvable, 119
- Resonance, 83
 - band, 197
 - condition, 78, 141
 - “deep”, 63
 - energy, 143
 - peak, 69, 145
 - phenomena, 71
- Resonances, 57, 103
 - and bound states, 103
 - and scattering states, 112
 - avoided crossings, 117–119
 - in transmission, 105
- Resonance
 - structure, 43
- Ripple in the continuum, 147
- Round trip, 78, 96
- Saddle-node bifurcation, 118
- Saturate, 65
- Scaling, 62
- Scattering
 - and avoided crossings, 117
 - boundary conditions for, 165
 - Bragg, 182
 - matrix, 20
 - potential, 20
 - resonances and bound states, 141, 144
 - state - resonant, 112
 - states - relation with bound states, 103
- Schrödinger equation, 1
 - time dependent, 1
 - time independent, 1
- Schwarz inequality, 131
- Secular equation
 - transfer matrix, 167
- Shape
 - barrier, 43
 - Gaussian, 95
 - of potential, 95
- Silicon, 215
- Similarity transformation, 30, 166
- Sine transform, 157, 159
- Single-well potential, 111
- Singularity
 - van Hove, 173
- S matrix, 20, 28
- Snapshot, 145
- Solar
 - cell, 215–216, 218
 - cell - band structure for, 221
 - constant, 214
 - irradiance, 214
 - panels, 214
- Solutions
 - particular, 9
- Spectra, 112